Developments of a multiplexer system for the High-Brilliance Neutron Source HBS

Marius Rimmler [a,b,*], Olaf Felden [b], Ulrich Rücker [c], Helmut Soltner [e], Paul Zakalek [c], Ralf Gebel [b], Thomas Gutberlet [c] and Thomas Brückel [a,d]

[a] *Lehrstuhl für Experimentalphysik IV C, RWTH Aachen, 52062 Aachen, Germany*
[b] *Institut für Kernphysik (IKP-4), Forschungszentrum Jülich GmbH, 52425 Jülich, Germany*
[c] *Jülich Centre for Neutron Science (JCNS-HBS), Forschungszentrum Jülich GmbH, 52425 Jülich, Germany*
[d] *Jülich Centre for Neutron Science (JCNS-2), Forschungszentrum Jülich GmbH, 52425 Jülich, Germany*
[e] *Zentralinstitut für Engineering, Elektronik und Analytik (ZEA-1), Forschungszentrum Jülich GmbH, 52425 Jülich, Germany*

Abstract. The High-Brilliance Neutron Source project (HBS) aims at developing a medium-flux accelerator-driven neutron source based on a 70 MeV, 100 mA proton accelerator. The concept optimizes the facility such that it provides high-brilliance neutron beams for instruments operating at different time structures. This can be realized by generating an interlaced proton pulse structure, which is unraveled and sent to three different target stations by a multiplexer system. In the following we present the developments of a multiplexer system at the JULIC accelerator at Forschungszentrum Jülich GmbH (FZJ), which serves as test facility for HBS. The main components of the JULIC multiplexer system are designed to be scalable to the HBS parameters.

Keywords: Neutron source, Accelerator-driven, Multiplexer

1. Introduction

Neutron scattering and neutron analytics are powerful tools for the observation of complex phenomena in condensed and soft matter science with impacts on innovations in our everyday life [1]. Low-energy accelerator-driven neutron sources represent a promising new type of neutron sources to fill the gap in neutron provision by the ongoing demise of older research reactors. Such sources can provide a healthy neutron eco-system and complement facilities such as the European Spallation Source (ESS) [2]. In low-energy accelerator-driven neutron sources, a primary proton beam below 100 MeV beam energy impinges on a metal target generating neutrons via nuclear reactions. The High-Brilliance Neutron Source project (HBS) aims to develop a pulsed accelerator-driven neutron source facility based on a high current 70 MeV linear proton accelerator, optimized to obtain a large neutron beam brilliane to source strength ratio and to be competitive with medium-flux[1] reactor neutron sources [3, 4]. The full-fledged HBS facility features simultaneous operation of different neutron instruments grouped around three target stations. Each station supplies a certain pulse structure fitting to the associated instruments. This will be realized by different proton beam timing schemes distributed to the target stations in order to obtain the optimal balance between wavelength bandwidth and resolution of the time-resolved neutron spectrum extracted from the thermal or cold neutron moderator according to the requirement of the individual experiment [5].

*Corresponding author. E-mail: m.rimmler@fz-juelich.de.

[1] Here, medium-flux refers to a thermal neutron flux in the order of $1 \times 10^{14}\,\mathrm{cm}^{-2}\,\mathrm{s}^{-1}$ at 1.5 Å neutron wavelength.

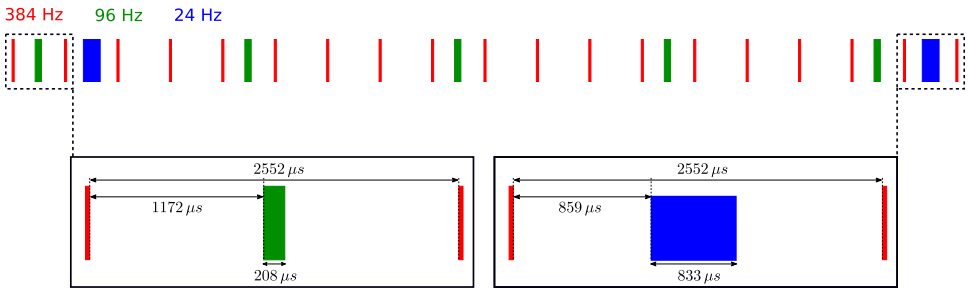

Fig. 1. Pulsing scheme of the primary proton beam of HBS. Red, green and blue pulses will be sent to the different neutron target stations. The lower part of the figure shows the time between subsequent pulses.

For HBS, a proton pulsing scheme as presented in Figure 1 is envisaged. The scheme is composed of three different pulse components with each component dedicated to an individual target station. With this, three target stations are operated independently at 24 Hz, 96 Hz and 384 Hz frequency and corresponding pulse lengths of 833 µs, 208 µs and 52 µs, which are coupled via a fixed duty cycle of 2 %. The multiplexer system is used in order to spatially separate the interlaced pulse components in Figure 1 and to send them to different target stations. The interlaced proton pulse sequence is generated with an electrostatic chopper, which is installed in front of the linear proton accelerator of HBS and behind an ECR ion source that operates in CW-mode [6, p. 57 f.]. The RF system of the HBS proton accelerator is pulsed according to the proton pulse sequence using solid state amplifiers [6, p. 50].

2. Layout

In order to unravel the multiplexed pulse structure in Figure 1, a multiplexer system following the concept in Figure 2 is used. The concept is based on a combination of a kicker and a septum magnet, which is a well established technique for spatial separation of ion beam pulses as used during injection or extraction processes of synchrotron accelerators [7]. The speciality of the multiplexer setup is that three different proton pulse components are separated symmetrically such that a newly developed Three-Field Septum Magnet (TFSM) is employed, which features three different magnetic field regions. Using a bipolar kicker magnet allows one to send individual proton pulse components separately towards the outer dipole field regions with different polarity of the TFSM, where these proton pulse components are further deflected into the respective beamline. When the kicker magnet is off, the proton beam is sent through a zero field region in the center of the TFSM such that is passes the multiplexer system without perturbation. The multiplexer setup is designed such that it can be combined with additional regular sector bending dipole magnets and quadrupole magnets to build an achromat for the beamlines, which emerge under an angle of 62° from the septum magnet. With this, the beam size further downstream the multiplexer setup is independent of the momentum uncertainty of the beam. The multiplexer setup will be designed for 70 MeV protons as utilized at the HBS facility [4]. The total length of the setup is approximately 10 m.

For the developments of individual components of the multiplexer setup such as the kicker and the TFSM, a test facility is provided at Forschungszentrum Jülich GmbH (FZJ). Here, the 45 MeV H^- cyclotron accelerator JULIC (Juelich Light Ion Cyclotron) supplies protons (stripping of H^-) to an experimental area with maximum 10 µA beam current [8, 9]. At this site, a test setup of the multiplexer as shown in Figure 3 is built. The conceptual design is based on the layout in Figure 2. However, the setup does not include additional sector bending dipole magnets and quadrupoles for achromatic beam optics due to spatial limitations. Furthermore, the test setup will supply only one target station, which is placed about 4 m downstream the multiplexer setup such that achromatic optics are not necessary for supplying the beam to the target. The test setup of the multiplexer uses a kicker magnet with 35 mrad deflection angle and a yoke length of 520 mm (610 mm effective length). The setup is combined with a Three-Field

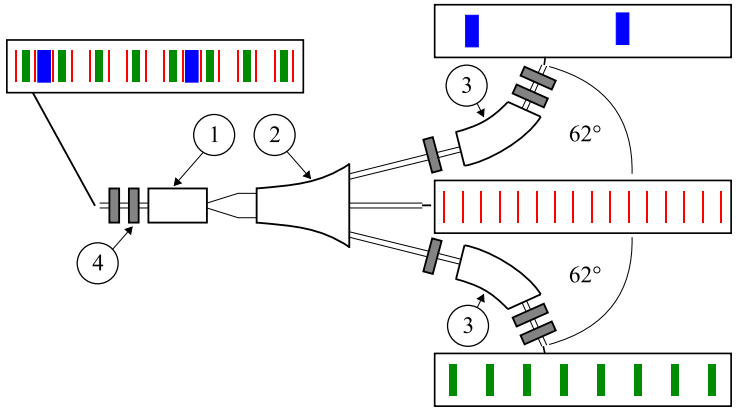

Fig. 2. Conceptual layout of the multiplexer system as realized at HBS and partly at JULIC. 1: bipolar kicker magnet, 2: septum magnet with three different field regions, i.e. Three-Field Septum Magnet (TFSM), 3: 45° sector bending magnet, 4: Quadrupole magnet (all in gray). The higher frequency proton pulse components are indicated in red, whereas the lower frequency proton pulse components are indicated in green and blue. After the multiplexer system, the interlaced pulse structure is unraveled into three beamlines separated by 62°. Note, that the multiplexer setup at JULIC does not include sector bending magnets (3) and quadrupole magnets (4) due to spatial limitations.

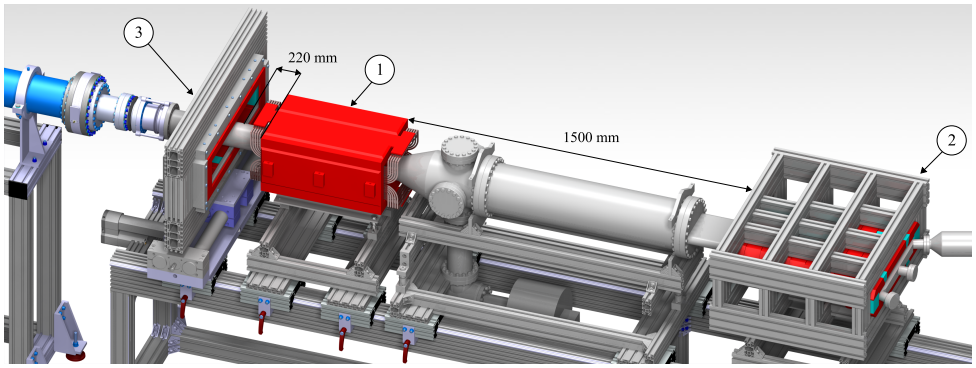

Fig. 3. Technical layout of the multiplexer system as realized at JULIC. The three main components of the multiplexer system are labeled. 1: kicker magnet, 2: Three-Field Septum Magnet (TFSM), 3: Three-Field Magnet (TFM) (labeling order according to the description in this work). The important dimensions, i.e. the distance from the kicker magnet to the TFSM and distance from the TFM to the kicker magnet, are indicated.

Septum Magnet (TFSM), which introduces a deflection of 265 mrad in the outer dipole field regions throughout a yoke length of 650 mm (697 mm effective length). The septum magnet features three different field regions, which are 62 mm apart[2] from each other at the front face of the magnet. After the septum magnet, three different beam ports for the straight and the deflected proton beam pulse components can be accessed. The multiplexer setup is completed by a so-called Three-Field Magnet (TFM) with yoke length of 140 mm (240 mm effective length) being capable of generating a beam deflection angle of 27 mrad, which is positioned in front of the kicker magnet. This magnet resembles a shorter version of the TFSM featuring two outer dipole field regions of opposite polarity and a centered zero field region. It is placed on a horizontally movable support. Depending on its horizontal position with respect to the beamline, the TFM acts either as static dipole magnet, which deflects the beam permanently into the outer dipole field regions of the septum magnet, or, if centerd, the TFM does not perturb the proton beam passing.

[2]Note, that the kicker magnet generates a beam deflection angle of 35 mrad, which results in an offset at the postion of the TFSM of 35 mrad · 1500 mm ≈ 52 mm. In addition the beam offset at the end of the kicker magnet with an effective length of 610 mm amounts for 610 mm · 35 mrad/2 ≈ 10 mm. Thus the total beam offset at the TFSM is approximately 62 mm. A similar consideration holds for the TFM.

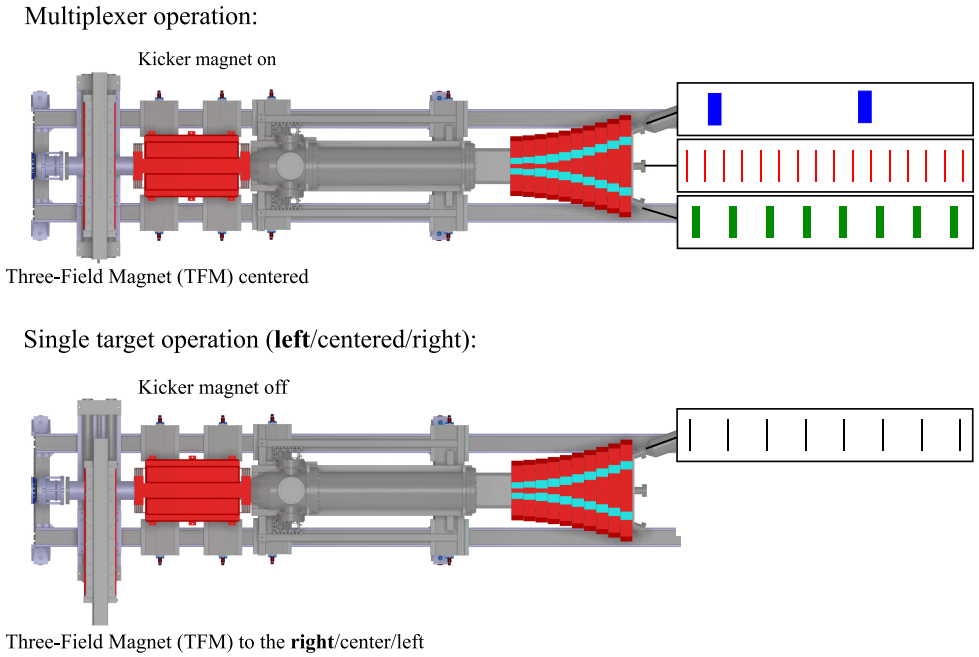

Fig. 4. Different operation modes of the multiplexer system at JULIC. The figure shows a top view of Figure 3. For multiplexer operation, i.e. parallel operation of all beamlines behind the TFSM, the bipolar kicker magnet is used and the TFM position is centered. For single target operation, i.e. operating one beamline behind the TFSM only, the kicker magnet is switched off and the TFM can be moved such that it introduces a dipole field to the proton beam thus steering the beam into one of the outer field regions of the TFSM. In the latter operation mode, the proton beam pulsing does not depend on the performance of the kicker magnet.

With this, the outer beam ports after the septum magnet can be operated individually without being limited to the performance of the kicker magnet, e.g. in CW-mode. The different operation scenarios are shown in Figure 4. Moreover, the development of the TFM serves as a proof of concept of the newly developed magnet technology employed in the TFSM design.

The components for the test setup at JULIC are designed to be scalable with respect to the proton energy and thus can be employed after redesign at HBS when going from 45 MeV to 70 MeV protons. For this, the magnet design and the corresponding magnetic field strength needs to be scaled to cope with the 26 % increase in magnetic rigidity of HBS with respect to the JULIC setup (as listed in Table 1). Concerning the beam quality, i.e. emittance, and the corresponding beam size at critical components such as the TFSM, the HBS conditions are more relaxed considering the up to 60 % smaller beam size for HBS in Table 1. This facilitates the design of the HBS components based on the JULIC developments.

3. Developments

The development of the main components of the multiplexer test setup in Figure 3 is presented in the following.

3.1. Kicker magnet

The kicker magnet, which is employed at the multiplexer test setup, is reused from the synchrotron COSY at Forschungszentrum Jülich GmbH, where it was used for injection. The magnet is a lumped inductance type kicker magnet. It is an electromagnet with 520 mm yoke length made from transformer sheets and 610 mm effective

Table 1
Ion beam parameters at the test setup at JULIC and at HBS. The parameters for the vertical plane are given in parentheses if they differ from the parameters in the horizontal plane. The variation of the dispersion function is along the reference orbit s, i.e. $\eta'_{x(y)} = \mathrm{d}\eta_{x(y)}/\mathrm{d}s$. Note, that the TWISS parameters β, α and the dispersion function η, η' as well as the rms beam size σ are presented at 145 mm in front of the TFSM of the respective multiplexer setup.

		JULIC	HBS
Particle		Proton	Proton
Beam energy	E/MeV	45	70
Beam rigidity	$(\mathrm{B}\rho)$/T m	0.98	1.23
Beam current	I/mA	0.01	100
norm. rms emittance	$\epsilon_{n,x(y)}$/mm mrad	3.1 (3.6)	1
beta function	$\beta_{x(y)}$/m	2.1 (4.0)	1.8 (13.2)
alpha function	$\alpha_{x(y)}$	-0.2 (2.2)	-0.3 (2.2)
dispersion function	$\eta_{x(y)}$/m	-1.3 (-1.2)	0
variation of dispersion function	$\eta'_{x(y)}$	0.07 (-0.04)	0
momentum uncertainty	$\delta/\%$	0.18	0.5
rms beam size	$\sigma_{x(y)}$/mm	5(7)	2(6)

length. The gap height is 180 mm. The magnet uses 20 windings of air-cooled copper coils to supply 57 mT at 409 A in order to generate 35 mrad deflection angle for 45 MeV protons. The magnet is installed at the experimental site and synchronized to the micropulsing, i.e. the proton pulse generation in the source beamline of the accelerator by an electrostatic deflector, of JULIC. During the testing of the magnet, the maximum magnet current was limited to 250 A and thus 35 mrad could not be achieved. However, tests were carried out with a special collimator system, which is installed 800 mm downstream the kicker magnet such that spatial separation of the different proton pulse components can be observed also for smaller kicker magnet deflection angles. Since the TFSM was subject to developments during the testing of the kicker magnet, the collimator system was used representing three target stations by independently monitoring the beam current at three different positions of the collimator system. The setup of collimator and kicker magnet is presented in Figure 5. For the first tests of the synchronization of kicker magnet and accelerator an unipolar power supply with limited performance in terms of rise, fall and flat top times, i.e. lower limits of 1 ms, 10 ms and 15 ms, respectively, of the magnet current as well as in terms of repetition rate of the current pulses, i.e. upper limit of 0.2 Hz, is used. The proton pulsing scheme is adjusted to consist of two different pulse components (Figure 1) with 20 Hz repetition rate and 5 ms pulse length for the pulse components, which are dedicated for the center part of the collimator, and 0.2 Hz repetition rate and 15 ms pulse length for the pulse components, which are foreseen to be deflected by the kicker magnet. Taking into account a delay of 50 µs for the time of flight of the protons from the chopper in the source beamline of the JULIC accelerator to the kicker magnet, the kicker magnet can be synchronized to only deflect the long proton pulse components, which is shown in Figure 6. The 15 ms long proton pulse components are deflected by the kicker magnet, which is observed by the dominant beam current signal on the right side of the collimator whereas the 5 ms pulse components go straight through the collimator shown by the similar behavior of the left and right side beam current signal on the collimator. The synchronization of the kicker magnet and the proton beam pulsing is established by using a pulse generator, which generates the multiplexed pulse structure through a chopper in the source beamline of the JULIC accelerator and simultaneously triggers the kicker magnet rise and fall. The measurement in Figure 6 has been carried out and averaged for 10 consecutive appearances of the 0.2 Hz proton pulse component, i.e. 50 s. Within this time interval, selective deflection of the 0.2 Hz proton pulse component without perturbation of the subsequent 20 Hz proton pulse components is observed. With the beam current measurement being triggered by the 0.2 Hz component, the 20 Hz proton pulse component prior to the deflected 0.2 Hz component could however not be investigated. This is subject to further systematic measurements of the multiplexer operation at JULIC. Furthermore, the current signal of the 0.2 Hz component on the right collimator plate seems to be decreasing within the last 5 ms of the pulse. It is currently being investigated if this can be caused by an early triggering of the kicker magnet

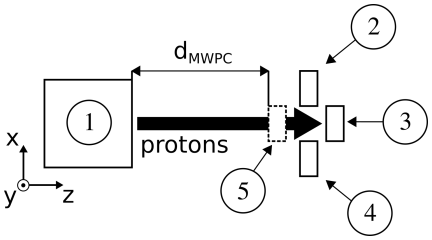

Fig. 5. Scheme of the kicker magnet synchronization test with the kicker magnet (1) and a special collimator system together with a beam cup providing three electrically insulated plates with the beam current on each plate being monitored independently. The different current measurements are performed at the left side of the collimator (2), the beam cup (3), and the right side of the collimator (4). A movable Multi Wire Proportional Chamber (MWPC - 5) at variable distance to the kicker magnet d_{MWPC} is used to measure the beam deflection angle.

Table 2

Performance of the kicker magnet and thus multiplexer at the JULIC test setup and at HBS in terms of rise t_{r}, fall t_{f} and flat top time t_{ft} of the kicker magnet and associated proton pulse compositions. The proton pulse compositions are classified by the maximum repetition rates of the straight f_{straight} and the deflected beam pulses $f_{\mathrm{deflected}}$ at the corresponding maximum possible duty cycle $\mathrm{dc}_{\mathrm{straight}}$ and $\mathrm{dc}_{\mathrm{deflected}}$, respectively. For the JULIC setup with performant power supply and for the HBS setup, where bipolar operation of the kicker magnet is possible, $\mathrm{dc}_{\mathrm{deflected}}$ and $f_{\mathrm{deflected}}$ apply to the duty cycle and repetition rate of the proton pulse components which are sent to the left and to the right field region of the septum magnet.

	JULIC	JULIC performant P.S.	HBS
t_{r}, t_{f}, t_{ft} in ms	1,10,15-50	0.5,0.5,0.1-10	0.5,0.5,0.1-10
f_{straight}, $f_{\mathrm{deflected}}$ in Hz	30,0.2	400,2×25	400,2×100
$\mathrm{dc}_{\mathrm{straight}}$, $\mathrm{dc}_{\mathrm{deflected}}$	4 %,1 ‰	4 %,2×0.2 %	4 %,2×2 %

fall slope. From the beam profile measurement in Figure 6, the beam deflection angle of the kicker magnet can be deduced by the beam centroid positions at different distances of the MWPC with respect to the kicker magnet to be $\Theta = -21.0(7)$ mrad. This is consistent with the expected beam deflection angle of the kicker magnet operating at 250 A, which is -21.8 mrad.

For HBS, the kicker magnet design will be similar to the magnet employed at JULIC. However, such kicker magnet requires water-cooled copper coils to work at 2 % duty cycle and larger repetition rate (96 Hz and 24 Hz as shown in Figure 1). The magnet gap height and number of turns should be chosen such that less than 500 A and 500 V are required from the power supply. This allows to develop a bipolar linearly regulated power supply with an IGBT switch to deal with the interlaced proton pulse structure with varying pulse widths and repetition rate. A bipolar performant power supply and an associated kicker magnet for HBS are currently under development at Forschungszentrum Jülich GmbH supplying 2 times 100 Hz repetition rate and less than 0.5 ms rise and fall times for the current pulses. The performant power supply will be installed for test purposes at kicker magnet of the JULIC test setup allowing an intermediate performance in terms of proton pulse compositions being restricted by thermal limitations of the air-cooled JULIC kicker magnet. The different scenarios and associated proton pulse compositions are listed in Table 2. For HBS, the proton pulse compositions, which will be made available are given in Figure 7. Note, that the repetition rate of the straight proton pulse components needs to be an integer multiple of the corresponding repetition rate of the deflected proton pulse components. One can see that for higher frequencies of the straight pulse components, the lower limit of deflected frequencies increases slightly due to the decreasing period length of the straight pulse components, i.e. a smaller time interval for the interlaced proton pulse component in Figure 1, and the large flat top times of the deflected pulse components with low frequency at fixed duty cycle.

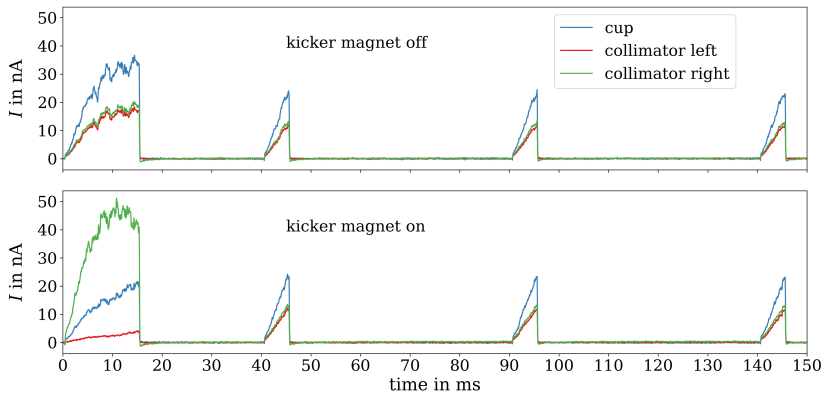

(a)

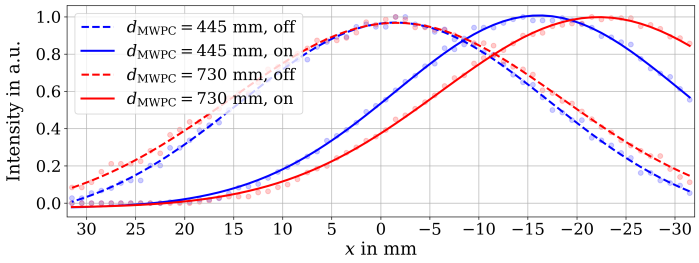

(b)

Fig. 6. (a): Beam current measurement of a multiplexed pulse structure consisting of a 15 ms long pulse with repetition rate 0.2 Hz and a 5 ms pulse with repetition rate 20 Hz. The beam current measurement is carried out with a setup as in Figure 5 installed in the experimental area at JULIC. The kicker magnet is at the exact position shown in Figure 3. The top and bottom plot show the multiplexed pulse structure with the kicker magnet being switched off and on, respectively. (b): Parallel horizontal beam profile measurement at the MWPC in Figure 5 triggered by the 0.2 Hz component at $d_{\mathrm{MWPC}} = 445\,\mathrm{mm}, 730\,\mathrm{mm}$. A gaussian fit is performed individually for all measurements with kicker magnet being off (dotted line) and on (solid line)

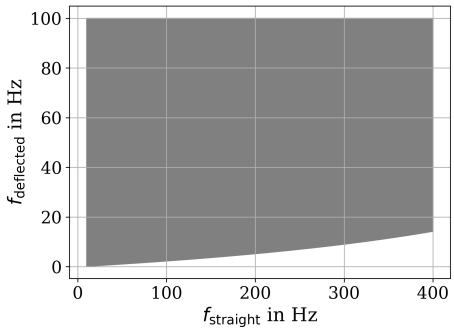

Fig. 7. Possible combinations of frequencies for the straight proton pulse components and the deflected proton pulse components emerging from the multiplexer envisaged at HBS with fixed duty cycle $\mathrm{dc}_{\mathrm{straight}} = 4\,\%$ and $\mathrm{dc}_{\mathrm{deflected}} = 2\,\%$ (see Table 2). Note, f_{straight} needs to be an integer multiple of $f_{\mathrm{deflected}}$.

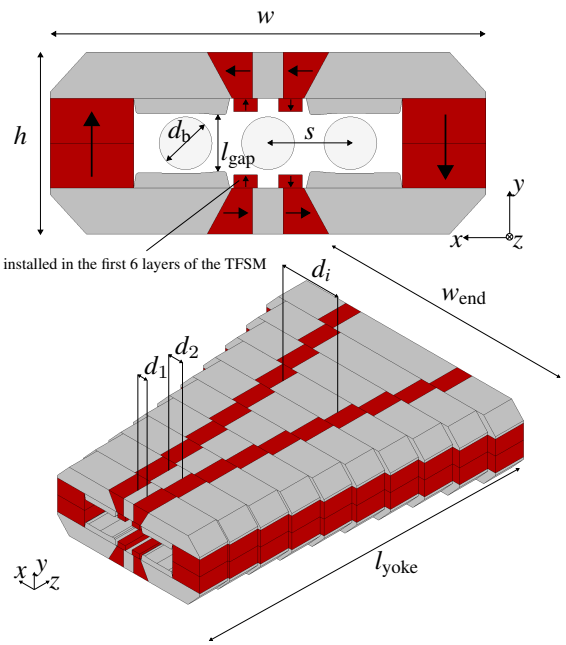

Fig. 8. Layout of the Three-Field Septum Magnet (TFSM) front face (top). The width of the front face is $w = 330$ mm (first layer in the bottom figure) and the height h amounts to 138 mm. The gap height $l_{gap} = 43$ mm allows to accommodate a beam diameter d_b of 40 mm. The septum front face is designed to obtain a separation of the beam spots of $s = 62$ mm. The red parts indicate SmCo magnets with $B_r = 1.1$ T, the gray parts show the magnet yoke material. The magnetization of the permanent magnets is indicated with arrows. The 4 small vertically magnetized compensator magnets are used in the first 6 layers of the TFSM as indicated. In the lower part of the figure, a 3D-drawing of the septum magnet with its individual layers and varying intermediate iron thicknesses d_i is shown. The yoke length of the magnet amounts to $l_{yoke} = 650$ mm while the maximum width at the end of the magnet is $w_{end} = 530$ mm. The origin of the coordinate system is in the geometric center of the magnet.

3.2. Three-Field Septum Magnet (TFSM)

The primary component of the multiplexer setup in Figure 2 as well as in the test setup in Figure 3 is the so-called Three-Field Septum Magnet (TFSM). This magnet enables the spatial separation of the different proton pulse components so that these can be directed into different beamlines and that the setup can be combined with additional quadrupole magnets within a compact design if required. For the multiplexer test setup, the TFSM needs to generate 265 mrad deflection angle throughout 650 mm yoke length requiring an integrated magnetic field of 260 mT · m for 45 MeV protons. Since the particle energy and particle species at low-energy accelerator-driven neutron sources are typically fixed, the magnetic field provided by the dipole field regions of the septum magnet is static. Therefore, the septum magnet is chosen to be based on permanent magnets. This is also advantageous since the septum magnet can be designed without electrical return conductors, which might have to be positioned in the aperture of the magnet. Thus the risk from radiation damages is reduced, which is especially important for the HBS facility with its large beam current of 100 mA. The technical design of the TFSM is shown in Figure 8. The magnet is based on horizontally and vertically magnetized rare earth SmCo magnets with a remanent magnetic flux density of $B_r = 1.1$ T combined with intermediate iron parts to guide the magnetic field lines. The arrangement of two large vertically magnetized permanent magnets on the outsides together with four horizontally magnetized trapezoidal permanent magnets in the center allows to generate two dipole field regions on the left and on the right side of the magnet with opposite polarity. In Figure 8, where the origin of the coordinate system is placed in the geometric center of the magnet, a dipole field region with $B_y > 0$ is obtained for $x = -62$ mm and symmetrically $B_y < 0$ is obtained for $x = 62$ mm. In the center, a zero field region with $B_y = 0$ is obtained. All field regions extend

by 20 mm to both sides in order to accommodate a beam with 40 mm diameter. In order to maintain a zero field region in the center of the magnet, four additional small vertically magnetized permanent magnets are employed at the entrance of the septum magnet to compensate the stray field from the outer dipole field regions. The septum magnet is designed to generate a deflection angle of 265 mrad throughout 650 mm yoke length, and therefore the aperture of the magnet has to be adapted in order to match the trajectory of the particles in the outer dipole field regions. This is realized by segmenting the septum magnet into ten layers. For each layer, the centered iron parts are adjusted in their corresponding width d_i ($1 \leqslant i \leqslant 10$) to fit the magnet aperture to the particle trajectory, which is shown in Figure 8 (bottom). The individual layers are then mounted onto each other by connections from the magnet yoke to an aluminium support frame similar to the construction of the TFM in Figure 11. A mock-up of such support structure for the TFSM is indicated in Figure 3. For this purpose, additional holes will have be drilled into the magnet yoke material. For the TFM in Figure 11, the addition of holes to the yoke did not have an effect on the field quality of the magnet and thus this is not considered in the following simulations. In addition to the positioning of the individual layers of the magnet, the horizontal positions of the small vertically magnetized compensator magnets (shown in Figure 8 top) are optimized individually in the first six layers. In the last four layers, these compensator magnets are not required as the horizontal separation of the different magnetic field regions is sufficiently large. The position of the compensator magnets is varied such that field homogeneity of the central zero field region according to

$$\max\left(\left|\int B_y(x,0)\mathrm{d}l - \int B_y(0,0)\mathrm{d}l\right|\right) \tag{1}$$

is optimal, i.e. the maximum deviation of the integrated magnetic field at $y = 0$ ($\int B_y(x,0)\mathrm{d}l$) within $-10\,\mathrm{mm} \leqslant x \leqslant 10\,\mathrm{mm}$ (within 4 horizontal rms beam widths and thus 95.45 % of the beam intensity according to Table 1) from the centroid position of the beam in the zero field region is minimized. With this, the results in Figure 9 are obtained. Here, the deviation of the integrated magnetic field in the central zero field region from the centered zero crossing according to Equation 1 amounts to 4 mT m. Similar to Equation 1, the field homogeneity for the outer field regions can be calculated according to

$$\max\left(\left|\frac{\int B_y(x+\Delta x(z),0)\mathrm{d}l - \int B_y(\Delta x(z),0)\mathrm{d}l}{\int B_y(\Delta x(z),0)\mathrm{d}l}\right|\right), \tag{2}$$

with $\Delta x(z)$ being the z-dependent beam centroid position in the outer field regions or integration planes in Figure 9. With this, the field homogeneity in the outer field regions for $-10\,\mathrm{mm} \leqslant x \leqslant 10\,\mathrm{mm}$ amounts to 1 %. The integrated field in the outer field regions of the septum magnet (Figure 9) is $274\,\mathrm{mT}\cdot\mathrm{m}$ which is about 5 % larger than the initially envisaged $260\,\mathrm{mT}\cdot\mathrm{m}$.

However, the beam is still well contained inside the septum magnet as shown by particle tracking studies in Figure 10 carried with the particle tracing module of the FEM code *Comsol* [10]. The TWISS parameters, which define the initial horizontal beam size, are taken from Table 1. To study the effect of all three field regions on the particle beam, three different beams are implemented in the simulation with the outer beams tilted accordingly to simulate the deflection angle introduced by the kicker magnet and to serve the outer field regions of the septum magnet. The particle tracking is carried out with 2.5×10^4 particles per beam. The deflection angle of the outer beams behind the TFSM in Figure 10 is 317 mrad instead of the initially planned 300 mrad to fit the geometry in Figure 3. The 6 % larger deflection angle can be compensated by reducing the magnetic field in the last layer of the septum magnet by the addition of iron shields, which is currently being investigated. The beam quality degradation during propagation through the TFSM is presented in Table 3 in terms of the emittance. Here, it can be seen that the maximum emittance growth amounts to 30 %. Note, that space charge effects have not been considered in the particle tracking study since the maximum beam current at JULIC is 10 µA at 45 MeV proton beam energy and

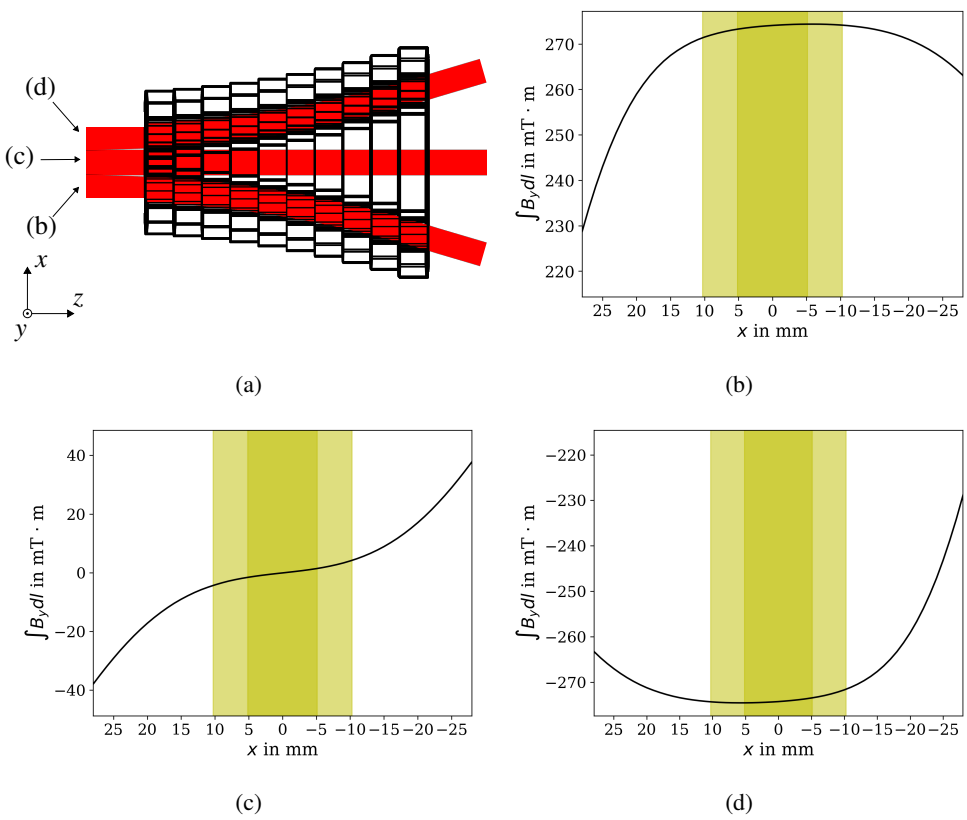

Fig. 9. (a): Integration planes (xz-planes at $y = 0$) for the calculation of the horizontal distribution of the integrated magnetic field of the septum magnet in Figure 8. The integration planes follow the expected beam trajectories with the integration limits along z from -525 mm to 525 mm. (b)-(d): Integrated vertical magnetic field $\int B_y \mathrm{d}l$ versus x as indicated in (a). In each integration plane a horizontally centered co-moving cartesian coordinate system is used. The expected extent of the proton beam according to Table 1 is indicated by the yellow shaded area (dark yellow: 2 rms beam widths, light yellow: 4 rms beam widths).

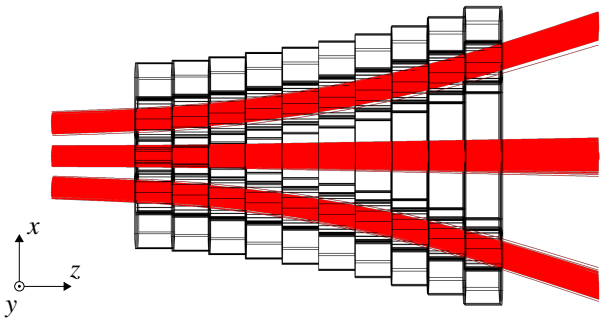

Fig. 10. Particle tracking of 45 MeV protons through the septum magnet for different settings of the kicker magnet with each setting serving a different field region of the septum magnet. The simulated transmission through all three field regions is above 99.998 %.

Table 3
Horizontal and vertical emittances of the proton beam in front of the TFSM and behind the TFSM. All three beam trajectories, i.e. left ($x > 0$), centered and right ($x < 0$), as shown in Figure 10 are investigated.

		145 mm in front of the TFSM	145 mm behind the TFSM		
			left	centered	right
hor. rms emittance (with dispersion)	$\epsilon_{\mathrm{disp.},x}$/mm mrad	10.2	12.7	13.4	11.8
vert. rms emittance (with dispersion)	$\epsilon_{\mathrm{disp.},y}$/mm mrad	15.9	15.4	16.6	15.4

thus space-charge-induced defocusing effects are negligibly small.

The operation of the TFSM under vacuum conditions for the proton beam is realized by inserting a custom-designed vacuum chamber into the aperture of the magnet. The TFSM design can be scaled from 45 MeV protons at JULIC to 70 MeV protons at HBS by increasing the number of layers in Figure 8 to enlarge the integrated magnetic field. Then, the aperture of the magnet needs to be adapted to follow the slightly different trajectories of particles at HBS proton energies with respect to the setup at JULIC. The development of the HBS TFSM is currently ongoing. Preliminary design studies suggest an arrangement with 945 mm yoke length, which is segmented into 15 layers. The magnetic dipole field in the outer field regions of the HBS TFSM is planned to be slightly smaller than for the JULIC TFSM, which facilitates the design as the fringe field effects from neighbouring field regions are reduced.

3.3. Three-Field Magnet (TFM)

As presented in Figure 3, a horizontally movable Three-Field Magnet (TFM) is employed in the test setup of the multiplexer at JULIC in order to operate all beam ports and thus potential target stations independently of the kicker magnet performance. With the TFM being used, the kicker magnet is off and the proton pulse composition for a certain beam port is only limited by the micropulsing, i.e. the electrostatic deflector in the source beamline of the accelerator JULIC (as shown in Figure 4). Apart from its use to complement the kicker magnet, the TFM is a proof of principle of the three-field permanent-magnet-based technology employed in the septum magnet and shown in Figure 8. The dimensions of the TFM are shown in Figure 11. The magnet is designed to enclose a vacuum beam tube with an outer diameter of 104 mm, which is the typical beam tube size used in the experimental area of the multiplexer test setup. Moving the setup in Figure 11 along x allows one to bring different field regions to the beam position. The magnet is designed to supply a dipole field region with $B_y > 0$ at $x = -230$ mm and $B_y < 0$ at $x = 230$ mm as well as a zero field region at $x = 0$. The respective field regions of the magnet extend horizontally by 30 mm on both sides, which is the expected beam size at the position of the magnet. The yoke length of the magnet is set to be 140 mm, which allows one to generate an integrated field of 33 mT · m. The effective length of the magnet is 240 mm with a maximum vertical magnetic flux density of 137 mT. From the geometry of the setup in Figure 3, an integrated field of the TFM of 26 mT · m is required, which is about 20 % smaller than the actual integrated magnetic field of the magnet. The magnet is deliberately designed to supply a larger integrated field than geometrically required to account for manufacturing inaccuracies, which can come from uncertainties of the remanent flux density of the permanent magnets employed. After manufacturing and measurements of the magnetic flux density distribution have been carried out to proof the working concept of the three different field regions, the integrated field is adjusted by iron sheets, which follow the cross section of the magnet to fit the geometrically required strength. Figure 12 shows a magnetic field measurement of the TFM in the centered xz-plane at $y = 0$ with the origin of the coordinate system being the geometrical center of the magnet in Figure 11. It can be seen that the three different field regions are clearly provided by the magnet design with a maximum dipole field in the outer field regions of up to 140 mT. The cut at $z = 0$ in Figure 12 shows a good agreement between measurement and simulation with the measured vertical magnetic field $B_{\mathrm{y,m}}$ being approximately 1.5 % stronger than the simulated field $B_{\mathrm{y,sim.}}$ in the outer dipole field regions of the TFM. The measured field homogeneity similar to Equation 2 in the outer field regions of the TFM is 1.4 %. In the centered field region, the integrated field deviates by maximum 1.3 mT m from the zero crossing in the center of the magnet (similar to Equation 1).

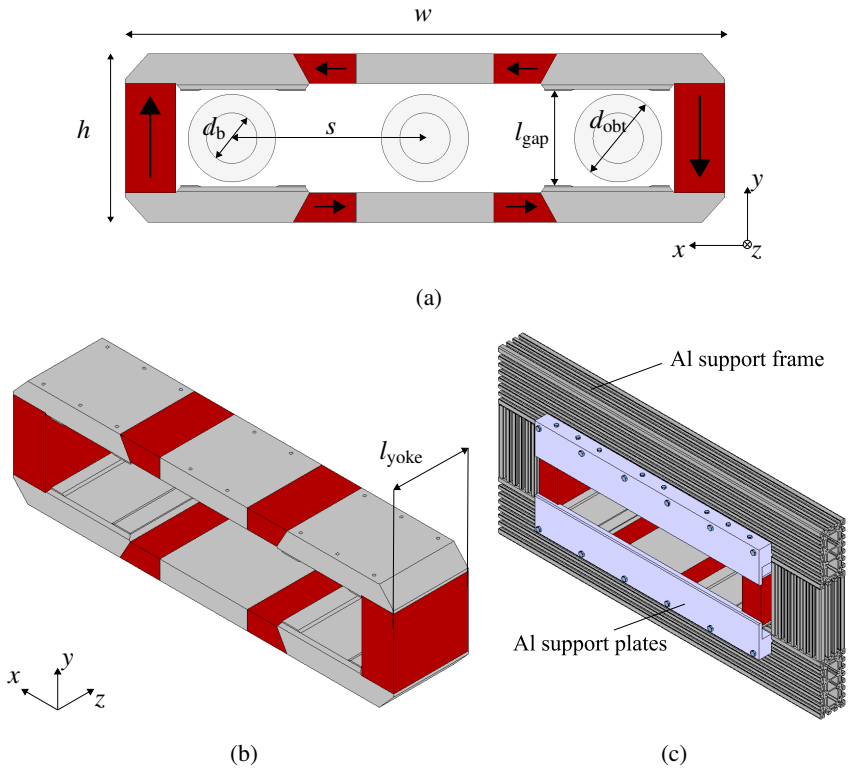

Fig. 11. Layout of the Three-Field Magnet (TFM). (a): The width of the front face is $w = 714$ mm and the height h amounts to 200 mm. The gap height $l_{gap} = 112$ mm allows to accommodate a beam tube with outer diameter $d_{obt} = 104$ mm. The expected beam diameter is $d_b = 60$ mm. The separation of the beam spots is $s = 230$ mm. The red parts indicate SmCo magnets with $B_r = 1.1$ T, the gray parts show the magnet yoke. The magnetization of the permanent magnets is indicated with arrows. (b): 3D-drawing of the TFM. The length of the magnet is $l_{yoke} = 140$ mm. (c): Full TFM setup with a customized Al support structure. Al support plates are mounted on the magnet yoke and connected to an Al support frame, which stabilizes the structure. The origin of the coordinate system is in the geometric center of the magnet.

4. Conclusion

In this work, we have shown the conceptual layout of a multiplexer system based on a kicker-septum magnet combination, which will be used at the High Brilliance Neutron Source HBS. With this system, different instruments at different target stations with different pulse lengths and repetition rates can be operated simultaneously. The key components of such a multiplexer system are developed and tested at a test facility for HBS, which is located at the cyclotron accelerator JULIC at Forschungszentrum Jülich GmbH. The components of the multiplexer test setup are designed to be scalable to HBS requirements, i.e. from 45 MeV protons at JULIC to 70 MeV protons at HBS. For the multiplexer test setup at JULIC, logics in terms of a kicker magnet being synchronized to the proton pulsing of the accelerator JULIC have been established to unravel a multiplexed pulse structure. Future upgrades of the power supply of the kicker magnet and of the kicker magnet itself being based on water-cooled coils will allow to perform experiments with the final pulse structure envisaged at HBS as shown in Figure 1. To introduce three different beamlines as intended by the multiplexer, a newly developed septum magnet is presented which features three different field regions. This Three-Field Septum Magnet (TFSM) is based on SmCo permanent magnets and has a scalable layered structure. The performance of the magnet is presented in terms of particle tracking of particles with corresponding energy and horizontal beam size. Furthermore, a prototype of the TFSM technology, i.e. a Three-Field Magnet (TFM), is shown which will be used additionally as switchable dipole magnet to perform multiplexer operation without limitations by the kicker magnet performance at the JULIC test setup.

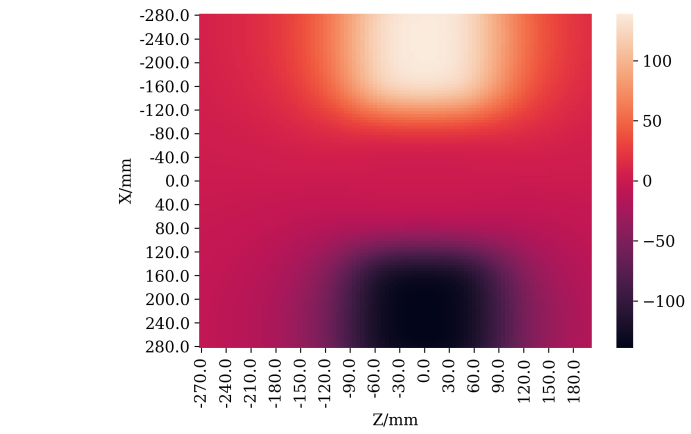

(a)

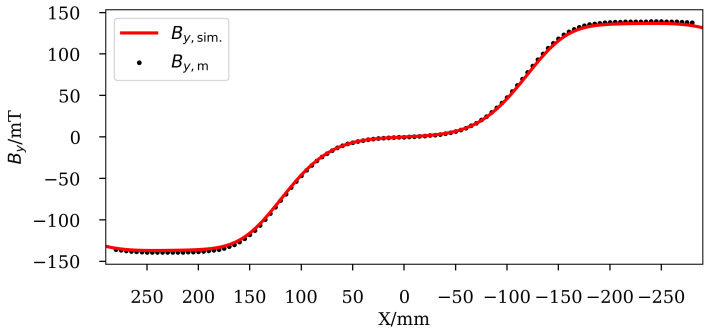

(b)

Fig. 12. (a): Measured vertical magnetic flux density B_y in the central xz-plane, i.e. $y = 0$ in Figure 11, in mT. (b): Cut from (a) at $z = 0$ with the simulated and measured vertical magnetic flux density $B_{y,\text{sim.}}$ and $B_{y,\text{m}}$, respectively.

Magnetic measurements of the TFM show the working concept of the magnet technology employed at the TFSM.

In summary, the key component of the multiplexer setup, i.e. the scalable Three-Field Septum Magnet (TFSM) has been developed for the test setup at JULIC and first tests with multiplexed beam at the test setup have been carried out paving the way for future multi-target operation with different neutron beam pulse structures at JULIC. For the consequential implementation of such multiplexer at HBS, further developments are required aiming for detailed designs of the respective components considering the HBS beam parameters and for a concept of the integration of the multiplexer setup into the proton beam transport while taking into account the large average beam power of 300 kW at HBS.

Acknowledgements

The authors are grateful to N.-O. Fröhlich and Y. Valdau for their strong support during the beam time for the kicker magnet tests. In addition, the authors acknowledge the help of C. Grates in the magnetic measurements of the Three-Field Magnet.

References

[1] E.N.S. Association, Neutrons for science and technology, Technical Report, 2017.

[2] ESFRI Physical Sciences and Engineering Strategy Working Group, Neutron Landscape Group, *ESFRI Scripta* **I** (2016).

[3] U. Rücker et al., The Jülich high-brilliance neutron source project, *The European Physical Journal Plus* **131** (2016), 19.

[4] P. Zakalek et al., High-brilliance neutron source project, *J. Phys.: Conf. Ser.* **1401** (2020), 012010.

[5] M. Rimmler et al., Proton beam multiplexer developments for multi-Target operation at the High-Brilliance Neutron Source HBS, *EPJ Web Conf.* **231** (2020), 02002.

[6] T. Brückel et al., Conceptual Design Report Jülich High Brilliance Neutron Source (HBS), Technical Report, Forschungszentrum Jülich GmbH, 2020.

[7] M.J. Barnes, J. Borburgh, B. Goddard and M. Hourican, Injection and extraction magnets: septa, 2011.

[8] W. Bräutigam et al., H- operation of the cyclotron JULIC as injector for the cooler synchrotron COSY-Jülich, *IOP* **654** (1999).

[9] O. Felden et al., Recent extensions of JULIC for HBS investigations, *Proc. Cyclotrons'19* (2019), 196–199.

[10] C. Inc., COMSOL multiphysics v. 5.6 - particle tracing module.